Electron-impact study of an NCO molecule using the *R*-matrix method

Savinder Kaur* and K. L. Baluja
Department of Physics and Astrophysics, University of Delhi, Delhi-110007, India
(Received 1 April 2012; published 3 May 2012)

We have carried out a comprehensive study of electron impact on an open shell NCO molecule by using the *R*-matrix method. Elastic (integrated and differential), momentum-transfer, excitation, and ionization cross sections, along with effective collision frequencies over a wide electron temperature range (500–30 000 K) have been presented. The target states are represented by including correlations via a configuration interaction formalism. The results of the static-exchange, correlated 1-state and 13-state close-coupling approximation are presented. Our study has detected five core excited shape resonances in the 13-state model. All calculations are done in the C_{2v} point group. We also detect a stable bound state of NCO^- of $^1A_1$ symmetry having configuration $\ldots 7a_1^2, 1b_1^2 2b_1^2, 1b_2^2 2b_2^2$ with a vertical electronic affinity value of 3.035 eV which is in good agreement with the experimental (adiabatic) value of 3.609 ± 0.0005 eV. The ionization cross sections are calculated using the binary-encounter-Bethe model in which molecular orbitals at self-consistent Hartree-Fock level are used to calculate kinetic and binding energies of the occupied molecular orbitals. For scattering calculations we have used partial waves up to $l = 4$ to represent the continuum electron in our *R*-matrix approach. A Born top-up procedure is invoked for dipole allowed transitions to account for the contribution of partial waves higher than $l = 4$ to obtain converged cross sections.

DOI: 10.1103/PhysRevA.85.052701 PACS number(s): 34.80.Bm, 34.80.Gs, 34.80.Ht

I. INTRODUCTION

We have performed a theoretical calculation of electron scattering from the NCO molecule. This molecule presents a feature in which each constituent atom is an open shell atom. The ground states of N, C, and O atoms have $2p^3$, $2p^2$, and $2p^4$ electronic configurations, respectively, giving rise to spin states of a quartet and triplet nature. There is considerable interest for the ionic isomers NCO and CNO in interstellar ices [1]. However, much effort has been devoted to the study of NCO^- on its spectroscopic property. The molecular cyanate NCO^- ion is used as a reagent in organic and inorganic synthesis and as an agent to calibrate the pressure in solids. The NCO^- anion is of considerable interest both in solution as well as the gas-phase chemistry.

Bradforth *et al.* [2] measured the ultraviolet photoelectron spectra of NCO^- and deduced the adiabatic electron affinity of the NCO molecule to be 3.609 ± 0.005 eV. Wight and Beauchamp [3] calculated a value of electronic affinity as 3.62 ± 0.2 eV from their measured NCO^- proton affinity using literature heats of formation for ΔH_f^o (HNCO) and ΔH_f^o (NCO).

Leonard *et al.* [1] reported an adiabatic electron affinity of 3.636 eV with zero-point energy correction. They showed that only the electronic ground state $X\,^1\Sigma^+$ of the NCO^- was stable with respect to ionization. In NCO the HOMO is a π orbital corresponding to a bonding combination of $2p_N$ and $2p_C$ atomic orbitals with an antibonding combination of $2p_C$ and $2p_O$ atomic orbitals. The additional electron of NCO^- totally fills this π molecular orbital. Svendsen *et al.* [4] calculated the adiabatic electron affinity for NCO to be 3.57 eV using the GAUSSIAN98 program package at the $B3LYP/6-311+G(2d)$ level of theory. Koch and Frenking [5] reported the adiabatic electronic affinity of 3.74 eV.

Our work uses the *ab initio* *R*-matrix method to study the low-energy electron scattering of the linear open shell NCO molecule in the fixed-nuclei approximation. The calculations use the UK molecular *R*-matrix code [6,7]. The *R*-matrix method provides cross sections at a large number of scattering energies efficiently. It includes correlation effects and gives an adequate representation of several excited states of the molecule [8]. Our interest lies in the low-energy region ($\leqslant$10 eV) where high-level but few-channel methods such as the *R*-matrix method work best. The incoming electron can occupy one of the many unoccupied molecular orbitals or can excite any of the occupied molecular orbitals as it falls into another one. These processes give rise to the phenomenon of resonances forming a negative molecular ion for a finite time before the resonance decays into energetically open channels. Below the threshold of the first vibrational channel, the energy loss is due to rotational excitations, which is very important for polar molecules where the cross section becomes enormous. The binary-encounter-Bethe (BEB) ionization cross sections [9,10] are also computed. The BEB cross sections depend on energy (kinetic and binding), the occupation number of the occupied molecular orbitals of the target, and the energy of the incident electron. The electron-scattering calculations are performed at the static-exchange (SE) level and close-coupling approximation, by including 1- and 13-target states, namely, the 1-state (CI 1-state) and 13-state close-coupling approximation.

II. METHOD

A. Theory

In the *R*-matrix theory [11,12] the configuration space of the scattering system is divided into an inner and an outer region. Both the regions are treated differently in accordance with

*Also at SGTB Khalsa College, Department of Physics, University of Delhi; sk_savinder2005@yahoo.co.in; kl_baluja@yahoo.com

the different interactions in each region. Once the scattering electron leaves the inner region, the other target electrons get confined to the inner region.

In the present work the R-matrix boundary radius dividing the two regions was chosen to be $12a_0$ centered at the NCO center of mass. This sphere encloses the entire charge cloud of the occupied and virtual molecular orbitals included in the calculation. At $12a_0$, the amplitudes of the molecular orbitals are less than $10^{-6}\, a_0^{-3/2}$. However, the continuum orbitals have finite amplitudes at the boundary. Inside the R-matrix sphere, the electron-electron correlation and exchange interactions are strong. Short-range correlation is important to describe the resonances. The behavior of the differential cross sections at small scattering angles is dictated by the dipole interaction (if present) and long-range polarization.

A multicentered configuration interaction (CI) wave-function expansion is used in the inner region. The calculation in the inner region is similar to a bound-state calculation, which involves the solution of an eigenvalue problem for $(N+1)$ electrons in the truncated space, where there are N target electrons and a single scattering electron. Most of the physics of the scattering problem is contained in this $(N+1)$ electrons bound-state molecular structure calculation. Outside the sphere, only long-range multipolar interactions between the scattering electron and the various target states are included. Since only direct potentials are involved in the outer region, a single center approach is used to describe the scattering electron via a set of coupled differential equations. The R matrix is a mathematical entity that connects the two regions. It describes how the scattering electron enters the inner region and how it leaves it. In the outer region, the R matrix on the boundary is propagated outward [13,14] until the inner region solutions can be matched with asymptotic solutions, thus yielding the physical observables like cross sections. We include only the dipole and quadrupole moments in the outer region.

In the polyatomic implementation of the UK molecular R-matrix code [6,7], the continuum molecular orbitals are constructed from atomic Gaussian-type orbitals (GTOs) using basis functions centered on the center of gravity of the molecule. The main advantage of GTOs is that integrals involving them over all space can be evaluated analytically in closed form. However, a tail contribution is subtracted to yield the required integrals in the truncated space defined by the inner region [6].

The target molecular-orbital space is divided into core (inactive), valence (active), and virtual orbitals. The target molecular orbitals are supplemented with a set of continuum orbitals, centered on the center of gravity of the molecule. The continuum basis functions used in polyatomic R-matrix calculations are Gaussian functions and do not require fixed boundary conditions. First, target and continuum molecular orbitals are orthogonalized using Schmidt orthogonalization. Then symmetric or Löwdin orthogonalization is used to orthogonalize the continuum molecular orbitals among themselves and remove linearly dependent functions [6,15]. In general and in this work, all calculations are performed within the fixed-nuclei approximation. This is based on the assumption in which electronic, vibrational, and rotational motions are uncoupled.

In the inner region, the wave function of the scattering system consisting of the target plus scattering electron is written using the configuration interaction (CI) expression

$$\Psi_k^{N+1} = A \sum_i \phi_i^N(x_1, \ldots, x_N) \sum_j \xi_j(x_{N+1}) a_{ijk} + \sum_m \chi_m(x_1, \ldots, x_N, x_{N+1}) b_{mk}, \quad (1)$$

where A is an antisymmetrization operator, x_N is the spatial and spin coordinate of the Nth electron, ϕ_i^N represents the ith state of the N-electron target, ξ_j is a continuum-orbital spin coupled with the scattering electron, and k refers to a particular R-matrix basis function. Coefficients a_{ijk} and b_{mk} are variational parameters determined as a result of the matrix diagonalization.

The first sum runs over the *thirteen* target states included in the present calculation, which are represented by a CI expansion. It accounts for one electron in a continuum state with the remaining electrons in a target state. To obtain reliable results, it is important to maintain a balance between the N-electron target representation, ϕ_i^N, and the $(N+1)$ electron-scattering wave function. The summation in the second term of Eq. (1) runs over configurations χ_m, where all electrons are placed in target occupied and virtual molecular orbitals. The choice of appropriate χ_m is crucial in this [16]. These are known as L^2 configurations and are needed to account for orthogonality relaxation and for correlation effects arising from virtual excitation to a higher electronic state that are excluded in the first expansion. The basis for the continuum electron is parametrically dependent on the R-matrix radius and provides a good approximation to an equivalent basis of orthonormal spherical Bessel functions [17].

We have used $55a_1$, $36b_1$, $36b_2$, and $23a_2$ continuum orbitals. The target and the continuum orbitals of a particular symmetry form an orthonormal set in the inner region; for example, the $8a_1$ orbitals of the target and $55a_1$ orbitals of the continuum are orthonormal to each other. The CSFs in the second term in Eq. (1) were constructed by allowing the scattering electron to occupy any of the target occupied or virtual orbitals. This term is responsible for the polarization effects in the 1-state CI calculation also.

B. NCO target model

The NCO radical is a linear, open shell molecule with 15 electrons and a ground-state electronic configuration of $1\sigma^2 \ldots 7\sigma^2 1\pi^4 2\pi^3$ in its natural symmetry. The double zeta plus polarization (DZP) Gaussian basis set [18] were used, contracted as (9,5,1)/(4,2,1) for the N atom, (9,5,2,2)/(4,2,1,1) for the C atom, and (9,5,1)/(4,2,1) for the O atom. The diffuse basis functions with an exponent smaller than 0.1 were omitted as they would extend outside the R-matrix box.

The optimized geometry in C_{2v} symmetry has the coordinates of N $= -1.253369A^\circ$, C $= -0.03794A^\circ$, and O $= 1.25173A^\circ$. We optimized the ground-state geometry at the Hartree-Fock level using the Gaussian GO3 package [19]. The sets of occupied and virtual orbitals were obtained by the self-consistent-field results (SCF) calculation for the ground state of the NCO molecule. This calculation yields occupied

TABLE I. NCO molecular-orbital binding $|B|$, average kinetic U energies (in eV), and occupation number N for the double zeta plus polarization (DZP) basis set at equilibrium geometry in C_{2v} symmetry.

Molecular orbital	$\|B\|$	U	N
$1a_1(1\sigma)$	562.53	794.63	2
$2a_1(2\sigma)$	425.91	602.28	2
$3a_1(3\sigma)$	311.33	436.05	2
$4a_1(4\sigma)$	41.12	75.36	2
$5a_1(5\sigma)$	34.37	59.81	2
$6a_1(6\sigma)$	21.22	71.60	2
$7a_1(7\sigma)$	17.13	55.51	2
$1b_1(1\pi)$	18.78	49.20	2
$2b_1(2\pi)$	12.92	51.20	2
$1b_2(1\pi)$	17.78	50.90	2
$2b_2(2\pi)$	7.47	48.34	1

orbitals up to $7a_1$, $2b_1$, and $2b_2$. The binding energies for the NCO molecule in the C_{2v} symmetry are tabulated in Table I.

The experimental value of ionization energy is 11.76 eV as reported in the Computational Chemistry Comparison and Benchmark Database (CCCBDB) [20]. The SCF calculations do not provide a good representation of the target states. The CI calculations were performed, which resulted in the lowering of the ground state and excited states. Also, the correlation introduced provides a better description of the target wavefunction and excitation energies. The SCF ground-state energy for NCO molecule is −167.14989 a.u. while our CI ground-state energy gets lowered to −167.2297 a.u., which is lower than that of Koch and Frenking [5], who calculated a value of −167.1289 a.u. This is due to the inclusion of more correlation effects in our calculations.

In the CI model, six frozen electrons were distributed in the $1a_1^2 2a_1^2 3a_1^2$ configuration and the remaining 15 electrons are allowed to move freely in eight molecular orbitals $4a_1 \ldots 7a_1$, $1b_1 2b_1$, and $1b_2 2b_2$. In our model we allow single as well as double excitations from the Hartree-Fock occupied orbitals to any one of the available virtual orbitals. There are also some selected triple excitations included, for example, $7a_1 \rightarrow 8a_1$, $2b_1 \rightarrow 3b_1$ and $2b_2 \rightarrow 3b_2$. The vertical electronic affinity (VEA) was computed using bound-state calculations by including the continuum electron basis functions centered at the origin. The stable bound state of NCO^- was calculated having a VEA value of 3.035 eV in good agreement with the 3.609 ± 0.005 eV experimental value [2]. This stable state of NCO^- can also be inferred from the highly negative unoccupied $2b_2$ molecular orbital with an energy of −7.47 eV.

The dipole moment is 0.36437 a.u. or $0.9255D$ while the components of the quadrupole moments Q_{20} and Q_{22} are 3.45599 and 0.88027 a.u., respectively, in the CI 13-state model. A good description of the extra electron requires a one-particle basis set augmented by a diffuse function as well as functions of high angular momentum.

In Table II, we list the dominant configuration, the transition moments N, the number of configuration state functions (CSFs), and the vertical excitation energies for the target states. The excited states are formed by the excitation of an electron from the occupied a_1, b_1, b_2, and a_2 orbitals to the vacant orbitals. In the R-matrix approach it is computationally convenient to use the same set of basis functions for all the target states. This is also a source of certain discrepancies in the target thresholds.

C. Scattering model

We have included 13 target states, taking five roots each in the $^2B_2$ and $^2B_1$, two roots in $^2A_1$, and one root in $^2A_2$ symmetries in the trial wave function describing the electron plus target system. Calculations were performed for doublet scattering states with A_1, A_2, B_1, and B_2 symmetries. Continuum orbitals up to the g partial wave ($l = 4$) were represented by Gaussians centered at the molecule center of gravity [17].

Due to the presence of the long-range dipole interaction, the elastic cross sections are formally divergent in the fixed-nuclei

TABLE II. Dominant configuration, transition moments (in a.u.), the number N of configuration state functions (CSFs), and vertical excitation energies (in eV) for the target states of the NCO molecule.

State C_{2v}	Dominant configuration	Transition moments	N	Vertical excitation energy
$X\ ^2B_2$	$(\ldots 6a_1^2 1b_1^2 1b_2^2), 7a_1^2 2b_1^2 2b_2^1$	0.3644[a]	7260	0.0000
$1\ ^2B_1$	$(\ldots)7a_1^2 2b_1^1 2b_2^2$	–	7260	0.0074
$1\ ^2A_1$	$(\ldots)7a_1^1 2b_1^2 2b_2^2$	0.2800	7364	3.1272
$2\ ^2B_2$	$(\ldots)7a_1^2 2b_1^2 3b_2^1$	0.3575	7260	5.1108
$2\ ^2B_1$	$(\ldots)7a_1^1 3b_1^1 2b_2^2$	–	7260	5.1109
$2\ ^2A_1$	$(\ldots)8a_1^1 2b_1^2 2b_2^2$	0.1460	7364	7.6633
$3\ ^2B_1$		–	7260	8.3549
$3\ ^2B_2$		0.0095	7260	8.3555
$4\ ^2B_1$		–	7260	9.0929
$4\ ^2B_2$		0.0011	7260	9.0930
$5\ ^2B_1$		–	7260	9.7922
$5\ ^2B_2$		0.0138	7260	9.7950
$1\ ^2A_2$		0.2413	7156	10.2693

[a]Represents the dipole moment.

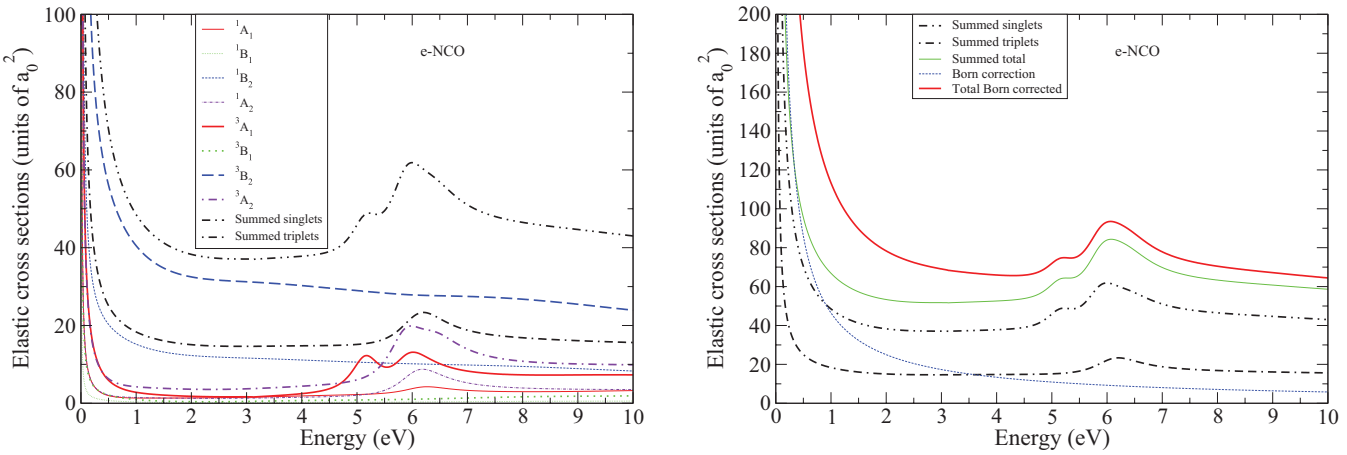

FIG. 1. (Color online) Elastic cross sections of the electron impact on the NCO molecule in the 13-state model. (a) Thin solid curve, $^1A_1$; thin dotted curve, $^1B_1$; thin dashed curve, $^1B_2$; thin dashed dotted curve, $^1A_2$; thick solid curve, $^3A_1$; thick dotted curve, $^3B_1$; thick dashed curve, $^3B_2$; thick dashed dotted curve, $^3A_2$; double dashed single dotted, summed singlets; double dotted single dashed, summed triplets. (b) Double dashed single dotted, summed singlets; double dotted single dashed, summed triplets; thin solid line, summed total; dashed line, Born correction; thick solid line, total Born corrected.

approximation as the differential cross section is singular in the forward direction. To obtain converged cross sections, the effect of rotation must be included along with a very large number of partial waves.

The effects of partial waves with $l > 4$ were included using a Born correction via a closure approach [21,22]. This correction is applied at the cross-section level at all energies. Our partial g-wave cross section using the R-matrix method nearly coincided with the g-wave and Born results in the entire scattering energy region. This establishes the correctness of our procedure to use Born correction beyond the g-partial wave.

The maximum number of coupled channels in our scattering calculation is 83. The number of CSFs for a typical singlet scattering symmetry is around 60 450, while for the triplet scattering it is around 61 370. Due to the small dipole moment (0.3643 a.u. or 0.9255D) of the ground state we have propagated the R matrix to a radius of $50a_0$. The propagated solutions at $50a_0$ are matched with the asymptotic boundary conditions yielding K matrices from which we can extract various types of cross sections using standard formulas.

III. RESULTS

A. Elastic and inelastic total cross sections

In Figs. 1(a) and 1(b) we present the elastic cross sections of electron impact on the NCO molecule in the CI 13-state model. In Fig. 1(a) we have shown the contribution of each symmetry. We detect resonances in $^3A_1$ symmetry at 5.22 eV with a width of 1.65 eV and at 6.00 eV with a width of 0.57 eV, in $^3A_2$ symmetry at 5.98 eV with a width of 1.02 eV, and in $^1A_2$ symmetry at 6.20 eV with a width of 1.11 eV. The resonance parameters are extracted from eigenphase sums matched to a Breit-Wigner profile [23]. All the four resonances are core excited resonances decaying to $2\,^2B_1$ and $2\,^2B_2$. In Fig. 1(b) we have plotted the summed cross sections from all the triplets and the singlet symmetries. In the SE calculation, exchange is included and the target molecule is not allowed to be perturbed and hence no polarization is included. In the CI 13-state model, exchange is included and the target molecule is allowed to be perturbed and hence polarization is included. In Fig. 1(b) we show the summed results of the singlets and the triplets. Born correction is applied to the summed total result and shown as the total Born corrected cross section.

The $^3A_1$ with configuration $(7a_1^2 2b_1 2b_2^2 3b_1)$ as well as $(7a_1^2 2b_1^2 2b_2 3b_2)$ decays to the $2\,^2B_1$ and $2\,^2B_2$ parent state, respectively, and thus is a core excited shape resonance. Further, $^3A_2$ with configuration $(7a_1^2 2b_1^2 2b_2 3b_1)$ decays to the $2\,^2B_2$ parent state while the $^1A_2$ with configuration $(7a_1^2 2b_1^2 2b_2 3b_1)$ decays to the $2\,^2B_2$ parent state, and thus both are also core excited shape resonances.

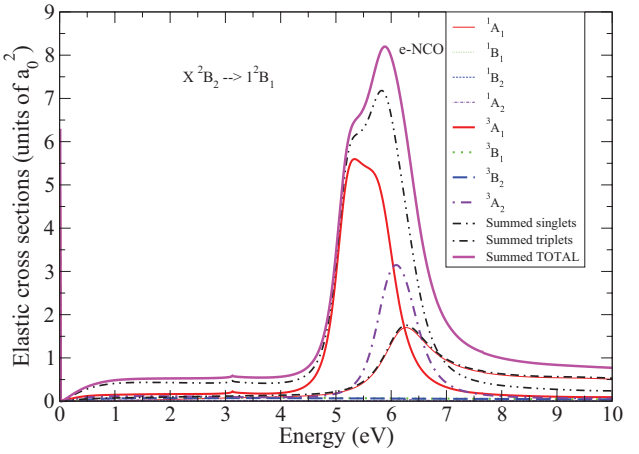

FIG. 2. (Color online) Electron-impact excitation cross sections from the ground $X\,^2B_2$ state of the NCO molecule to the $1\,^2B_1$ state in the 13-state model. Thin solid curve, $^1A_1$; thin dotted curve, $^1B_1$; thin dashed curve, $^1B_2$; thin dashed dotted curve, $^1A_2$; thick solid curve, $^3A_1$; thick dotted curve, $^3B_1$; thick dashed curve, $^3B_2$; thick dashed dotted curve, $^3A_2$; double dashed single dotted, summed singlets; double dotted single dashed, summed triplets; thickest curve, summed total.

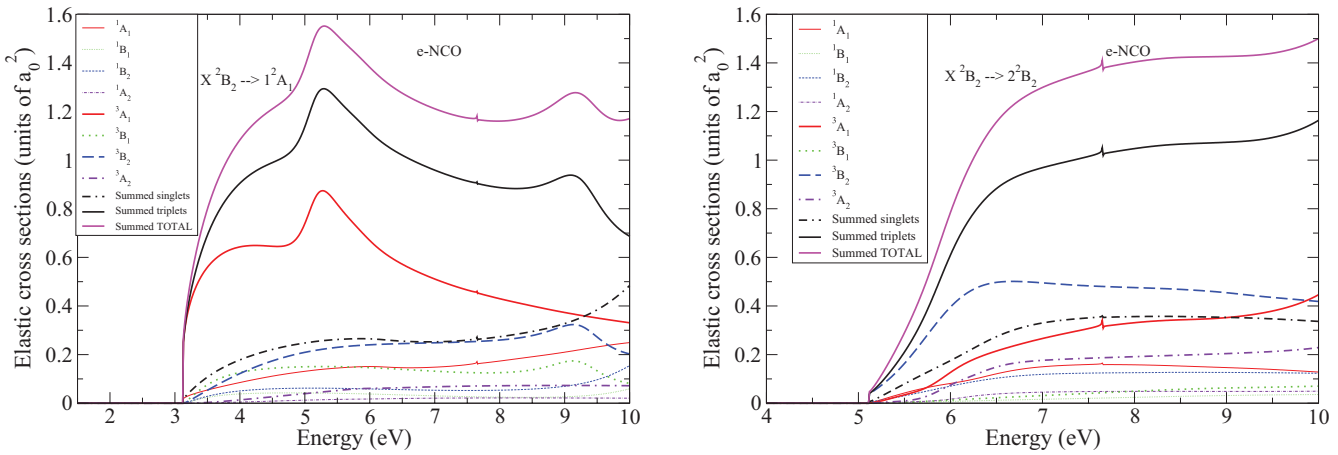

FIG. 3. (Color online) Electron-impact excitation cross sections from the ground $X\,^2B_2$ state of the NCO molecule to the (a) 1^2A_1 state and the (b) 2^2B_2 state in the 13-state model. Thin solid curve, $^1A_1$; thin dotted curve, $^1B_1$; thin dashed curve, $^1B_2$; thin dashed dotted curve, $^1A_2$; thick solid curve, $^3A_1$; thick dotted curve, $^3B_1$; thick dashed curve, $^3B_2$; thick dashed dotted curve, $^3A_2$; double dashed single dotted, summed singlets; double dotted single dashed, summed triplets; thickest curve, summed total.

In Fig. 2, we have shown excitation cross sections for the transition $X\ ^2B_2 \rightarrow 1\,^2B_1$. This is the not a dipole allowed transition. Peaks in $^3A_2$ and $^3A_1$ have been discussed in earlier figures. We see a peak at 6.22 eV in $^1A_1$ symmetry with a width of 2.25 eV. The $^1A_1$ with configuration $(7a_1^2 2b_1^2 2b_2 3b_2)$ decays to the $2\,^2B_2$ parent state and is also a core excited shape resonance. The mild signature of this resonance can also be seen at the same position in Fig. 1(a).

The highest occupied molecular orbital (HOMO) in C_{2v} symmetry is $2b_2$ with an orbital energy of -7.47 eV. In Figs. 3(a) and 3(b) we have shown the inelastic cross sections from the ground state $X\ ^2B_2$ to the first two dipole allowed states $1\,^2A_1$ and $2\,^2B_2$ whose vertical excitation thresholds along with their dominant configuration and the number of CSFs included in the CI expansion are given in Table II. In Fig. 3(a) the cross sections for $^3A_1$ symmetry are dominant. The peak in $^3A_1$ symmetry corresponds to the core excited shape resonance as discussed earlier. All other cross sections are small. In Fig. 3(b) the cross sections are nearly of the same range and none exhibit any particular resonance. In Figs. 4(a) and 4(b) the individual contributions of the singlets and the triplets as shown in Figs. 3(a) and 3(b) have been summed and the Born correction has been applied.

The transition in Fig. 5 is a spin-forbidden transition and depicts the $X\,^2B_2 \rightarrow 2\,^2B_1$ excitation cross section in which we also show the individual contributions of each scattering symmetry. Though the cross sections of the triplet symmetries are lower we notice again the peaks in $^3A_1$ at 5.84 eV and $^3A_2$ at 6.21 eV. These are core excited shape resonances.

Figure 6 depicts the $X\,^2B_2 \rightarrow 2\,^2A_1$ excitation cross section in which we also show the summed contributions of the singlets and the triplets. Born correction is applied but since the transition moment is only 0.1460 a.u. the contribution is negligible. The cross sections of the singlets rise monotonically and present no special feature in the cross sections.

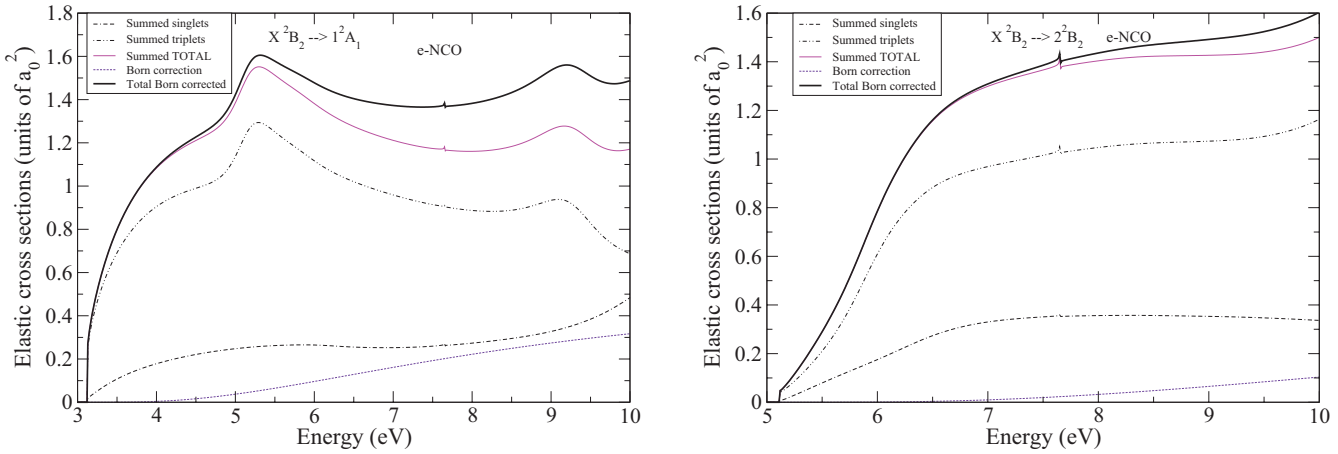

FIG. 4. (Color online) Electron-impact excitation cross sections from the ground $X\,^2B_2$ state of the NCO molecule to the (a) $1\,^2A_1$ (b)$2\,^2B_2$ state in the 13-state model after including the Born correction. Double dashed single dotted, summed singlets; double dotted single dashed, summed triplets; thin solid line, summed total; dashed line, Born correction; thick solid line, total Born corrected.

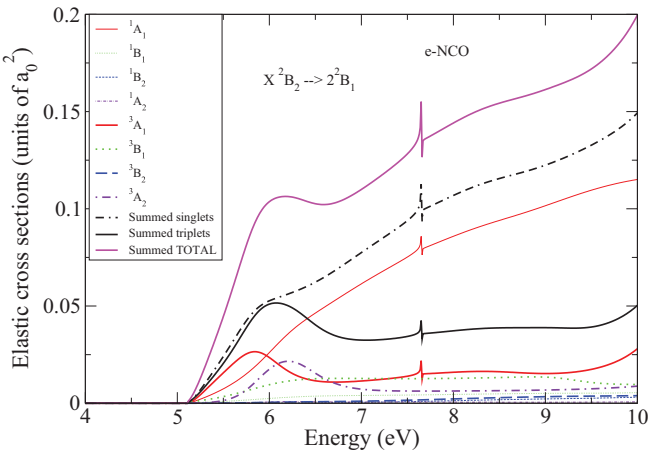

FIG. 5. (Color online) Electron-impact excitation cross sections from the ground $X\ ^2B_2$ state of the NCO molecule to the $2\ ^2B_1$ state in the 13-state model. Thin solid curve, $^1A_1$; thin dotted curve, $^1B_1$; thin dashed curve, $^1B_2$; thin dashed dotted curve, $^1A_2$; thick solid curve, $^3A_1$; thick dotted curve, $^3B_1$; thick dashed curve, $^3B_2$; thick dashed dotted curve, $^3A_2$; double dashed single dotted, summed singlets; double dotted single dashed, summed triplets; thickest curve, summed total.

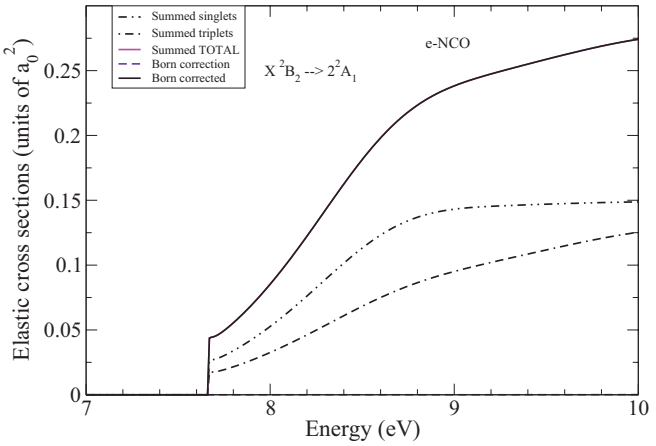

FIG. 6. (Color online) Electron-impact excitation cross sections from the ground $X\ ^2B_2$ state of the NCO molecule to the $2\ ^2A_1$ state in the 13-state model. Double dashed single dotted, summed singlets; double dotted single dashed, summed triplets; thickest curve, summed total; dashed line, Born correction; thick solid line, total Born corrected.

The resonance position E_r and the resonance width Γ_r parameters of the resonances yielded by 13-state close-coupling calculations are given in Table III.

B. Ionization cross section

The BEB cross section is rather sensitive to the ionization energy used in the calculation. The ionization energy used in our calculation is 11.76 eV, which is the experimental value obtained from CCCBDB. The molecular-orbital data used in the calculation of the BEB cross section are given in Table I. These molecular orbitals used in our CI model were obtained through an SCF calculation, which is used to calculate the BEB cross sections. The ionization cross section σ is obtained by summing over each orbital cross section σ_i, where

$$\sigma_i(t) = \frac{S}{t+u+1}\left\{\frac{1}{2}\left(1-\frac{1}{t^2}\right)lnt + \left[\left(1-\frac{1}{t}\right)-\frac{lnt}{t+1}\right]\right\}, \tag{2}$$

where $t = T/B$, $u = U/B$, and $S = 4\pi a_0^2 N(R/B)^2$. Here, R is the Rydberg energy, T is the kinetic energy of the incident electron, U is the orbital kinetic energy, N is the electron occupation number, and B is the binding energy of the orbital.

We have calculated the electron-impact ionization cross section of NCO by using the standard formalism of the binary-encounter-Bethe (BEB) model [9,10]. This formalism requires the binding energy and kinetic energy of each occupied molecular orbital in a molecular structure calculation. The parameter Q of the BEB formalism is set to unity. The BEB cross sections are given in Fig. 7 from threshold (11.76 eV) to 5000 eV. The cross section rises from threshold to a peak value of $4.62 A^{\circ 2}$ at 88.86 eV and then shows lnE/E behavior as E approaches higher values.

TABLE III. Resonance parameters of NCO.

Electronic configuration of resonant state	E_r (eV)	Γ_r (eV)	Type of resonance	Parent state
$^3A_1 : (\ldots)7a_1^2 2b_1^2 2b_2 3b_2$	5.2158	1.65	Core excited	$2\ ^2B_2$
$^3A_1 : (\ldots)7a_1^2 2b_1 2b_2^2 3b_1$	6.00248	0.57	Core excited	$2\ ^2B_1$
$^3A_2 : (\ldots)7a_1^2 2b_1^2 2b_2 3b_1$	5.977	1.02	Core excited	$2\ ^2B_2$
$^1A_2 : (\ldots)7a_1^2 2b_1^2 2b_2 3b_1$	6.1991	1.11	Core excited	$2\ ^2B_2$
$^1A_1 : (\ldots)7a_1^2 2b_1^2 2b_2 3b_2$	6.22	2.25	Core excited	$2\ ^2B_2$

C. Differential cross section

The evaluation of the differential cross section (DCS) provides a more stringent test for any theoretical model. The DCS for a general polyatomic molecule is given by the familiar expression

$$\frac{d\sigma}{d\Omega} = \sum_L A_L P_L(\cos\theta), \tag{3}$$

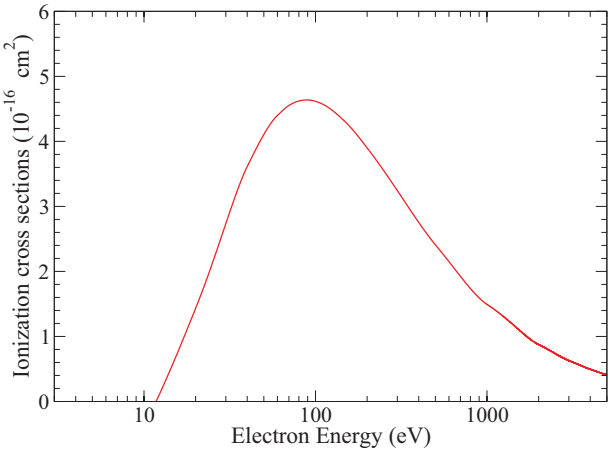

FIG. 7. (Color online) Electron-impact BEB ionization cross sections of the NCO molecule.

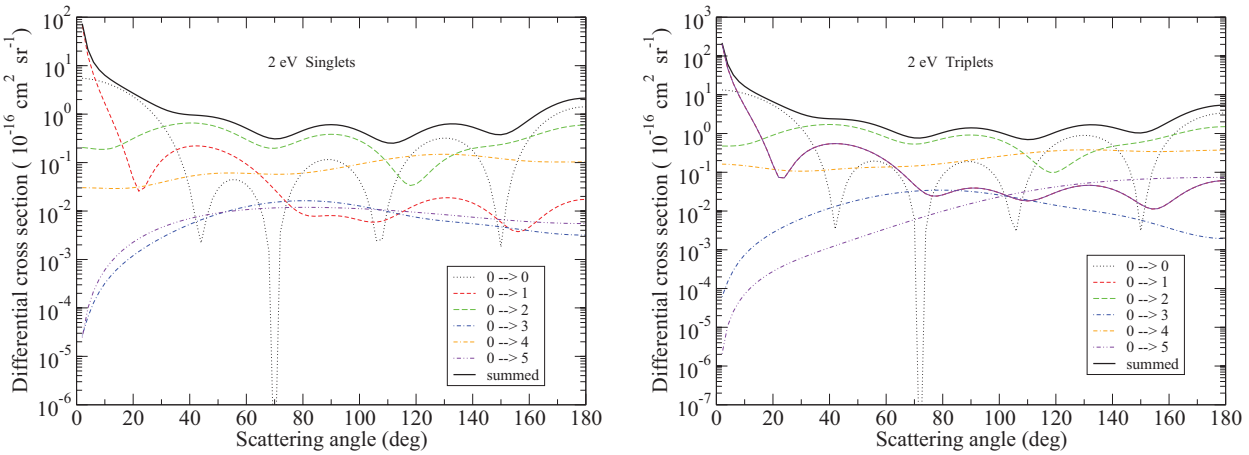

FIG. 8. (Color online) Electron-impact R-matrix rotationally resolved state-to-state ($J \rightarrow J'$) cross sections of NCO at 2 eV in the 24-state model: thin dotted curve, $0 \rightarrow 0$; thin dashed curve, $0 \rightarrow 1$; big dashed curve, $0 \rightarrow 2$; dash dotted curve, $0 \rightarrow 3$; double dash dotted curve, $0 \rightarrow 4$; double dot dashed curve, $0 \rightarrow 5$; thick curve, summed (over J') results. (a) Singlets. (b) Triplets.

where P_L is a Legendre function. The A_L coefficients have already been discussed in detail by Gianturco and Jain [24]. For the polar molecule this expansion over L converges slowly. We use the closure formula to accelerate the convergence of DCS:

$$\frac{d\sigma}{d\Omega} = \frac{d\sigma^B}{d\Omega} + \sum_L \left(A_L - A_L^B\right) P_L(\cos\theta). \tag{4}$$

The superscript B denotes that the relevant quantity is calculated in the Born approximation with an electron-point dipole interaction. The convergence of the series is now rapid since the contribution from the higher partial waves to the DCS is dominated by the electron-dipole interaction. The quantity $d\sigma^B/d\Omega$ for any initial rotor state $|J\tau\rangle$ is given by the sum over all the final rotor states $|J'\tau'\rangle$:

$$\frac{d\sigma^B}{d\Omega} = \sum_{J'\tau'} \frac{d\sigma^B}{d\Omega}(J\tau \rightarrow J'\tau'). \tag{5}$$

The expression for the state-to-state rotationally inelastic DCS, $d\sigma^B/d\Omega(J\tau \rightarrow J'\tau')$, for a spherical top, a symmetric top, and an asymmetric top molecule are given by Sanna and Gianturco [25]. We used the calculated rotational constant for NCO, which is $B = 0.3985892509\ \text{cm}^{-1}$ at the geometry used in the present calculation.

In Figs. 8(a) and 8(b) we show our calculated rotationally resolved differential cross section for electron scattering by NCO at the incident energy of 2 eV for the singlet and triplet symmetries separately. The scattering is dominated by the elastic component $0 \rightarrow 0$, the dipole component $0 \rightarrow 1$, and the quadrupole component $0 \rightarrow 2$. As J' increases the cross sections decrease; this shows that by $J' = 5$ we have obtained almost convergent results. In Fig. 9 we show DCSs which are obtained by summing the rotational cross sections for all processes $J = 0 \rightarrow (J' = 0 - 5)$ at selected energies of 2,4,7, and 10 eV. Further, we have used a weight factor of 1/4 for the summed singlets contribution and 3/4 for the summed triplets and plotted the DCS. The DCSs at all the energies show a steep rise as the scattering angle approaches zero. This is due to the dipolar nature of the target. Besides this, the data on DCS are further used to calculate the momentum-transfer cross section (MTCS) that weights the backward angle scattering. We have

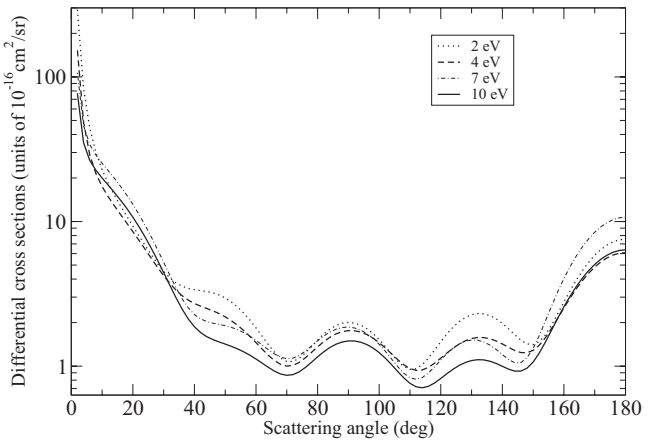

FIG. 9. Electron-impact R-matrix DCS of NCO differential cross sections in the 13-state model: dotted curve, 2 eV; dashed curve, 4 eV; dash dotted curve, 7 eV; solid curve, 10 eV.

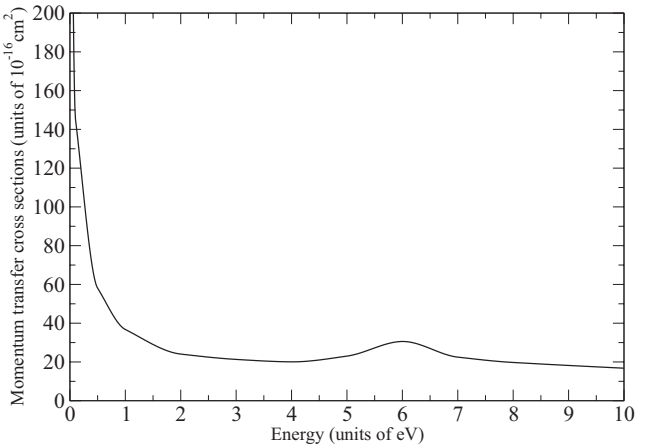

FIG. 10. Momentum-transfer cross sections of the NCO molecule ground-state, solid curve, 13-state result.

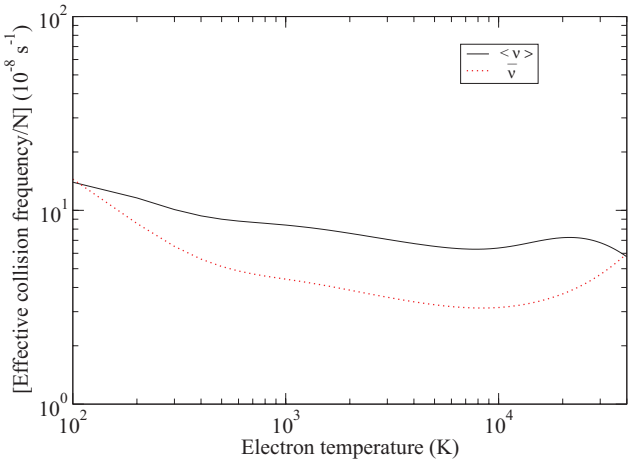

FIG. 11. (Color online) Effective collision frequency of the NCO molecule ground state: solid curve, $\langle \nu \rangle$; dotted curve $\bar{\nu}$.

calculated DCS by using the POLYDCS program of Sanna and Gianturco [25] that requires basic molecular input parameters along with K matrices evaluated in the R-matrix scattering calculation.

However, since the DCSs are not very sensitive to correlation effects (due to the polar nature of the molecule) for backward scattering, we expect our MTCS to be quite reliable, shown in Fig. 10 in the 1–10-eV range. It provides a useful input in solving the Boltzmann equation for the electron distribution function. From Fig. 10, we observe that MTCS decreases with increasing energy. The peak near 6 eV is due to the effect of resonances. In contrast to the diverging nature of DCS in the forward direction, MTCS shows no singularity due to the weighting factor $(1 - \cos\theta)$, where θ is the scattering angle. This factor vanishes as $\theta \to 0$. The MTCS is useful in the study of electrons drifting through a molecular gas.

D. Effective collision frequency of electrons

Using the MTCS data, we evaluated two types of the effective electron-NCO collision frequency $\langle \nu \rangle$ and $\bar{\nu}^{-1}$ (see Baille *et al.* [26]). These are given by the following expressions, in which it is assumed that the electrons follow a Maxwell-Boltzmann distribution:

$$\langle \nu \rangle = \frac{8}{3\pi^{1/2}} N \left(\frac{m_e}{2kT_e} \right)^{5/2} \int_0^\infty v^5 Q^m(v) e^{-\frac{m_e v^2}{2kT_e}} dv, \qquad (6)$$

and

$$\bar{\nu}^{-1} = \frac{8}{3\pi^{1/2} N} \left(\frac{m_e}{2kT_e} \right)^{5/2} \int_0^\infty \frac{v^3}{Q^m(v)} e^{-\frac{m_e v^2}{2kT_e}} dv. \qquad (7)$$

Here, N is the number density of molecules, m_e is the electron mass, k is the Boltzmann factor, T_e is the electron temperature, v is the velocity of the electron, and $Q^m(v)$ is the velocity-dependent MTCS. These are plotted in Fig. 11. These collision frequencies are related to transport properties like mean-free path, mobilities, and diffusion coefficients. These find applications in the study of electrons swarming through molecular gases.

IV. CONCLUSIONS

We have carried out a detailed study of electron impact on the linear open shell NCO molecule by using the R-matrix method. We have presented results for various types of cross sections. The vertical electronic affinity is in agreement with the experiment adiabatic electronic affinity. The data generated for MTCS have been fruitfully employed to calculate collision frequencies which are useful for the evaluation of transport coefficients. Our study has detected five core excited shape resonances in the 13-state model. The ionization cross section presented in the BEB model may be useful to experimentalists as resource data.

[1] C. Leonard, H. Gritli, and G. Chambaud, J. Chem. Phys. **133**, 124318 (2010).
[2] S. E. Bradforth, E. H. Kim, D. W. Arnold, and D. M. Neumark, J. Chem. Phys. **98**, 800 (1993).
[3] C. A. Wight and J. L. Beauchamp, J. Phys. Chem. **84**, 2503 (1980).
[4] A. Svendsen, M. O. A. El Ghazaly, and L. H. Andersen, J. Chem. Phys. **123**, 114311 (2005).
[5] W. Koch and G. Frenking, J. Phys. Chem. **91**, 49 (1987).
[6] L. A. Morgan, C. J. Gillan, J. Tennyson, and X. Chen, J. Phys. B **30**, 4087 (1997).
[7] L. A. Morgan, J. Tennyson, and C. J. Gillan, Comput. Phys. Commun. **114**, 120 (1998).
[8] J. Tennyson, J. Phys. B **29**, 1817 (1996).
[9] Y. K. Kim and M. E. Rudd, Phys. Rev. A **50**, 3954 (1994).
[10] W. Hwang, Y. K. Kim, and M. E. Rudd, J. Chem. Phys. **104**, 2956 (1996).
[11] *Atomic and Molecular Processes: An R-Matrix Approach*, edited by P. G. Burke and K. A. Berrington (Institute of Physics, Bristol, 1993).
[12] C. J. Gillan, J. Tennyson, and P. G. Burke, in *Computational Methods for Electron-Molecule Collisions,* edited by W. M. Huo and F. A. Gianturco (Plenum, New York, 1995).
[13] K. L. Baluja, P. G. Burke, and L. A. Morgan, Comput. Phys. Commun. **27**, 299 (1982).
[14] L. A. Morgan, Comput. Phys. Commun. **31**, 419 (1984).
[15] B. M. Nestmann, K. Pfingst, and S. D. Peyerimhoff, J. Phys. B **27**, 2297 (1994).
[16] J. Tennyson, J. Phys. B **29**, 6185 (1996).
[17] A. Faure, J. D. Gorfinkiel, L. A. Morgan, and J. Tennyson, Comput. Phys. Commun. **144**, 224 (2002).
[18] T. H. Dunning and P. J. Hay, in *Methods of Electronic Structure Theory*, edited by H. F. Schaefer, Vol. 2 (Plenum, New York, 1977).
[19] Guassian GO3 package, http://www.gaussian.com.
[20] NIST, Computational Chemistry Comparison and Benchmark Database, http://cccbdb.nist.gov.
[21] S. Kaur, K. L. Baluja, and J. Tennyson, Phys. Rev. A **77**, 032718 (2008).

[22] S. Kaur and K. L. Baluja, Phys. Rev. A **80**, 042701 (2009).
[23] J. Tennyson and C. J. Noble, Comput. Phys. Commun. **33**, 421 (1984).
[24] F. A. Gianturco and A. Jain, Phys. Rep. **143**, 347 (1986).
[25] N. Sanna and F. A. Gianturco, Comput. Phys. Commun. **114**, 142 (1998).
[26] P. Baille, J. S. Chang, A. Claude, R. M. Hobson, G. L. Ogram, and A. W. Yau, J. Phys. B **14**, 1485 (1981).